Imaging, Diagnosis, Prognosis

Clinical Cancer Research

Drug-Induced Vessel Remodeling in Bone Metastases as Assessed by Dynamic Contrast Enhanced Magnetic Resonance Imaging and Vessel Size Imaging: A Longitudinal *In vivo* Study

Tobias Bäuerle[1], Maximilian Merz[1], Dorde Komljenovic[1], Stefan Zwick[2], and Wolfhard Semmler[1]

Abstract

Purpose: The aim of this study was to assess the antiangiogenic treatment effects of zoledronic acid (ZA) and sunitinib malate (SM) noninvasively in experimental breast cancer bone metastases by dynamic contrast-enhanced magnetic resonance imaging (DCE-MRI) and vessel size imaging.

Experimental Design: Nude rats bearing bone metastases after inoculation of MDA-MB-231 breast cancer cells were treated with ZA (40 μg/kg weekly; n = 8 rats), SM (20 mg/kg daily; n = 8 rats), or their combination (ZA and SM; n = 8 rats) and compared with sham-treated controls (n = 10 rats). Vascular changes in bone metastases were longitudinally imaged *in vivo* using DCE-MRI [amplitude (A) and exchange rate coefficient (k_{ep})] and vessel size imaging [blood volume (BV) and vessel size index (VI)]. In addition, antiresorptive and antitumor changes were assessed in these lesions by flat-panel volumetric computed tomography as well as morphologic MRI and diffusion-weighted imaging.

Results: In bone metastases, significant changes in A, k_{ep}, BV, and VI in accordance with decreased blood volume and vessel permeability as well as with increased mean vessel diameters were observed after application of ZA and SM as compared with controls. In this longitudinal study, antiangiogenic changes preceded the inhibition of osteolysis and antitumor effects after treatment.

Conclusions: These results indicate vessel remodeling in breast cancer bone metastases on ZA and SM treatment and implicate substantial effects on imaging and treatment of malignant bone lesions. *Clin Cancer Res; 16(12); 3215–25. ©2010 AACR.*

Bone is among the most frequent locations of metastasis in patients with breast cancer. In these patients, bone marrow represents a fertile soil for cancer cells by homing factors that stimulate various processes in the development and progression of bone metastases such as tumor cell proliferation, bone resorption, and angiogenesis. Angiogenic factors in the bone marrow are essential for the cross-talk of osteoclasts, osteoblasts, and bone marrow endothelial cells. In patients with skeletal metastases, the expression of angiogenic factors was associated with osteoclast-mediated osteolysis and, vice versa, antiangiogenic therapy resulted in antiresorptive treatment response in these lesions (1–4). Recently, a close anatomic relation between capillaries and bone remodeling units consisting of osteoclasts and osteoblasts was observed in osteolytic lesions, indicating a possible interaction between angiogenesis and bone resorption (5). For these reasons, angiogenesis plays a crucial role in the pathogenesis of breast cancer bone metastasis, but the effect of the inhibition of angiogenesis is still unclear in these lesions.

Both antiangiogenic and antiresorptive effects were reported for bisphosphonates as current standard treatment for breast cancer bone metastases as well as for the tyrosine kinase inhibitor sunitinib malate (SM; ref. 6). On treatment with bisphosphonates including zoledronic acid (ZA), vascular endothelial growth factor (VEGF) was decreased in the blood of breast cancer patients (7). ZA was furthermore shown to inhibit proliferation of endothelial cells, to modulate endothelial cell adhesion and migration, as well as to reduce vessel sprouting (8, 9). The multitargeted receptor tyrosine kinase inhibitor SM inhibits important vascular targets such as VEGF receptor and platelet-derived growth factor receptor. SM has already been approved for the treatment of gastrointestinal stroma tumors and renal cell carcinomas, but was shown to exhibit strong antiangiogenic activities in many more primary tumors including breast cancer (10). Interestingly, SM has been reported to inhibit osteolysis in experimental

Authors' Affiliations: [1]Department of Medical Physics in Radiology, German Cancer Research Center, Heidelberg, Germany and [2]Department of Diagnostic Radiology, Medical Physics, University Hospital Freiburg, Freiburg, Germany

Corresponding Author: Tobias Bäuerle, Department of Medical Physics in Radiology, German Cancer Research Center, Im Neuenheimer Feld 280, 69120 Heidelberg, Germany. Phone: 49-6221-422569; Fax: 49-6221-422585; E-mail: t.baeuerle@dkfz.de.

doi: 10.1158/1078-0432.CCR-09-2932

Translational Relevance

The noninvasive imaging methods used in our study for assessment of antiangiogenic treatment response in experimental bone metastases, including dynamic contrast-enhanced magnetic resonance imaging (DCE-MRI) and vessel size imaging, can be applied to humans with such skeletal lesions accordingly. Translation of the presented results into the clinical situation is in particular facilitated as a regular MRI scanner for humans at 1.5 T was used, which is widely available.

The observed antiangiogenic effects of treatment with zoledronic acid and sunitinib malate in experimental bone metastases were associated with antiresorptive as well as antitumor effects and require further validation in clinical studies. When applying zoledronic acid and sunitinib malate in patients, DCE-MRI and vessel size imaging could be used for early and quantitative assessment of treatment response in malignant bone lesions.

breast cancer bone metastases (11, 12). However, the antiangiogenic effects of ZA and SM have not been studied in bone metastases.

For noninvasive assessment of angiogenesis, magnetic resonance imaging (MRI) techniques such as dynamic contrast-enhanced MRI (DCE-MRI) and vessel size imaging (VSI) can be applied to assess vascular changes such as vessel remodeling by the calculation of quantitative biomarkers (13, 14). DCE-MRI is widely used in preclinical cancer research as well as in oncologic patients, including applications in bone metastases, whereas VSI is a comparatively new technique (15, 16). The current standard to assess treatment response in breast cancer patients with bone metastases is the determination of tumor size in bone by MRI and computed tomography (CT; ref. 17). Furthermore, by detecting changes in cellularity, the apparent diffusion coefficient (ADC) from diffusion-weighted imaging (DWI) was found to be an imaging biomarker of early treatment response in bone metastases (18).

The aim of this study was to assess the antiangiogenic treatment effects of the bisphosphonate ZA and the receptor tyrosine kinase inhibitor SM in experimental breast cancer bone metastases using DCE-MRI and VSI, as well as the resulting antitumor and antiresorptive effects of these therapies by morphologic MRI, DWI, and flat-panel volumetric CT (VCT). To our knowledge, this is the first study to noninvasively investigate the antiangiogenic effects of ZA and SM in bone metastases *in vivo*.

Materials and Methods

Cell lines and culture conditions

The human estrogen-independent breast cancer cell line MDA-MB-231 was obtained from the American Type Culture Collection. Tumor cells were cultured routinely in RPMI 1640 (Invitrogen) supplemented with 10% FCS (Sigma). All cultures were kept under standard conditions (37°C, humidified atmosphere, 5% CO_2) and passaged two to three times a week to keep them in logarithmic growth.

Animal model and treatment

Experiments were approved by the governmental animal ethics committee (Regierungspräsidium Karlsruhe, Germany). Nude rats (RNU strain) were obtained from Harlan Winkelmann at the age of 6 weeks. They were housed at specific pathogen-free conditions in a mini-barrier system of the central animal facility under controlled conditions. For all procedures including tumor cell inoculation and *in vivo* imaging, rats were anesthetized with a mixture of nitrous oxide (1 l/min), oxygen (0.5 l/min), and isoflurane (1-1.5 vol%). For tumor cell inoculation, 10^5 MDA-MB-231 tumor cells were injected in the right superficial epigastric artery of nude rats as described previously (19). Resulting bone metastases were observed exclusively in the femur, tibia, and fibula of the right hind leg of these animals.

Nude rats (n = 34) bearing bone metastases were randomly distributed into four groups. After the initial imaging on day 0 (30 days after tumor cell injection; for details, see below), SM (SU-11248, Pfizer; n = 8, oral application of 20 mg/kg daily), ZA (Roche; n = 8, s.c. application of 40 μg/kg weekly), or their combination (n = 8; 20 mg/kg SM, oral application daily, and 40 μg/kg ZA, s.c. application weekly) was given to nude rats until the end of the observation time at day 25 after initiation of therapy and compared with untreated controls (n = 10, s.c. application of saline instead of SM or ZA).

In vivo imaging

In vivo imaging of experimental breast cancer bone metastases was done at day 0 (before initiation of therapies) as well as 5, 15, and 25 days after initiation of therapies using VCT and MRI as described previously (20, 21).

Flat-panel VCT. VCT imaging was done on a prototype flat-panel equipped volumetric computer tomograph (Volume CT, Siemens) with the following parameters: tube voltage, 80 kV; tube current, 50 mA; scan time, 51 seconds; rotation speed, 10 seconds; frames per second, 120; matrix, 512 × 512; and slice thickness, 0.2 mm.

Magnetic resonance imaging. MRI was done on a 1.5-T MR-scanner (Symphony, Siemens) using an appropriate home-built coil for radiofrequency excitation and detection (20, 21). The animals were imaged with the following sequences. (*a*) T2 weighted images: turbo spin-echo sequence [orientation, axial; TR, 3,240 ms; TE, 81 ms; matrix, 152 × 256; field of view (FOV), 53.4 × 90 mm^2; slice thickness, 1.5 mm; averages, 3; images, 15; scan time, 3:40 min]; (*b*) diffusion-weighted imaging: half-Fourier acquisition single-shot turbo spin-echo sequence (b = 0, 50, 100, 200, and 600 s/mm^2 through the largest diameter of the tumor; orientation, axial; TR, 4,000 ms; TE, 155 ms;

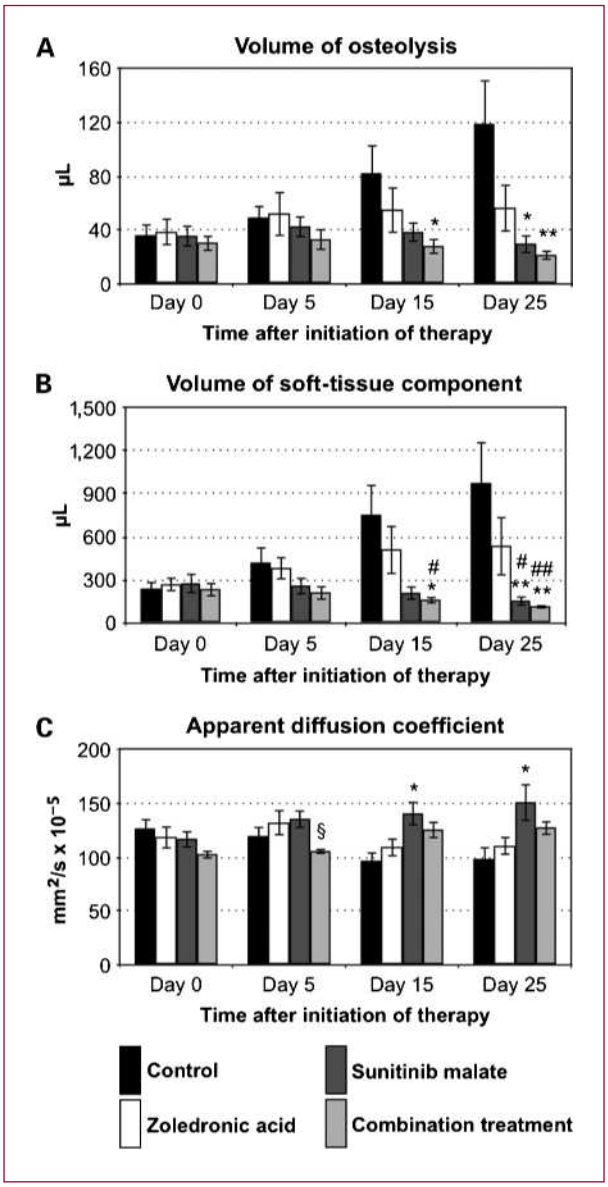

Fig. 1. A to C, study results of parameters acquired with VCT, morphologic MRI, and DWI from experimental bone metastases at days 0, 5, 15, and 25 after initiation of treatment. A, volumes of osteolytic lesions as imaged by VCT. B, volumes of soft-tissue components as imaged by morphologic MRI. C, ADC as imaged by DWI. Bars, SE. *, compared with the control group; #, compared with the ZA monotherapy group; §, between SM and combination treatment groups (*, #, and §, $P < 0.05$; ** and ##, $P < 0.01$).

matrix, 72 × 128; FOV, 45 × 80 mm^2; slice thickness, 2 mm; averages, 10; images, 15; scan time, 5 × 2:00 min); (*c*) dynamic contrast-enhanced imaging: saturation recovery turbo flash sequence (through the largest diameter of the tumor; orientation, axial; TR, 373 ms; TE, 1.86 ms; matrix, 192 × 144; FOV, 130 × 97.5 mm^2; slice thickness, 5 mm; measurements, 512; averages, 1; images, 512; scan time, 6:55 min) while infusing 0.1 mmol/kg Gd-DTPA i.v. (Magnevist, Schering) over a time period of 10 seconds; and (*d*) vessel size imaging: T2 weighted spin-echo sequences (TR, 6,000 ms; TE, 80 ms; matrix, 128 × 104; resolution, 0.5 × 0.5 × 1.5 mm^3; averages, 1; images, 40; scan time, 13:00 min) were acquired before and 3 minutes after i.v. administration of ultrasmall superparamagnetic iron oxide particles (200 µmol Fe/kg; Sinerem, Laboratoires Guerbet) as well as T2* weighted multigradient echo sequence (FLASH; TR, 320 ms; TE, 4.76-47.6 ms; matrix, 128 × 104; resolution, 0.5 × 0.5 × 1.5 mm^3; averages, 3; images, 108; scan time, 7:00 min) pre- and post-injection of the ultrasmall superparamagnetic iron oxide particles.

Postprocessing. The volumes (in microliters) of the osteolytic lesions and the soft-tissue components were determined on unenhanced VCT and magnetic resonance images by volumetry (The Medical Imaging Interaction Toolkit, Germany). For DCE-MRI, DWI, and VSI, regions of interest were drawn manually around the tumor lesion to determine the respective values for amplitude (*A*; arbitrary units), exchange rate constant (k_{ep}; 1/min), vessel size index (VI; µm), blood volume (BV; arbitrary units), and ADC (mm^2/s × 10^{-5}) in bone metastases. DCE-MRI data were postprocessed according to the pharmacokinetic two-compartment model of Brix et al. (22) and maps for the ADC were calculated as reported previously (20, 21). Pixel-based data analysis for VSI to obtain the parameters VI and BV was done on an analysis software built with the rapid prototyping software Rad-Builder (Siemens Corporate Research). Due to technical failure during measurement, the number of VSI measurements on days 0 and 5 was reduced for animals that received ZA (day 0, $n = 6$ and day 5, $n = 6$) and for control animals (day 0, $n = 5$ and day 5, $n = 6$). Motion correction of the images was not necessary as the tumor-bearing hind leg of animals was fixed on a plastic bedding during image acquisition.

Bone storage and histology

The lower limbs from each animal were excised at sacrifice (day 25) and processed as described previously (20). For immunohistochemical staining, the following antibodies were used: primary antibodies—rabbit polyclonal against rat collagen IV (Progen Biotechnik GmbH; dilution 1:50) and rat α-smooth muscle actin (mouse monoclonal, Sigma Aldrich; dilution 1:400); secondary antibodies—donkey anti-rabbit Texas red sulfonyl chloride (Jackson ImmunoResearch; dilution 1:100) and goat anti-mouse Cy2 (Jackson ImmunoResearch; dilution 1:50). The preparations were rinsed again with PBS, counterstained using 4′,6-diamidino-2-phenylindole (Serva), dried, and coverslipped.

After immunohistochemical staining, five FOVs from sections of five representative animals of each group were examined using a Leica microscope (DMRE) with an adapted digital camera (F-view XS, Soft Imaging System). On these sections, quantitative analysis of marker densities was done by calculating positive area fractions; mean vessel diameters were also measured using Analysis Software (cell^F, Olympus Soft Imaging Solutions). The microvessel

Table 1. Study results from longitudinal imaging (A, mean values of imaging parameters; B, comparison between study groups) and histology (C)

A

Imaging method	Group	Mean value			
		Day 0	Day 5	Day 15	Day 25
VCT: Volume of osteolysis (μL)	Control	36	49	82	119
	Zoledronic acid	39	52	55	57
	Sunitinib malate	36	43	38	30
	Combination treatment	31	33	28	21
MRI: Volume of soft-tissue component (μL)	Control	237	419	752	974
	Zoledronic acid	270	383	513	537
	Sunitinib malate	276	260	210	154
	Combination treatment	236	213	161	116
DWI: Apparent diffusion coefficient ($mm^2/s \times 10^{-5}$)	Control	127	120	97	99
	Zoledronic acid	119	132	110	111
	Sunitinib malate	117	136	141	151
	Combination treatment	103	106	126	128
DCE-MRI: Amplitude (arbitrary units)	Control	106	110	106	113
	Zoledronic acid	102	93	87	91
	Sunitinib malate	114	89	74	61
	Combination treatment	113	81	70	60
DCE-MRI: Exchange rate constant (1/min)	Control	51	47	51	49
	Zoledronic acid	43	38	39	29
	Sunitinib malate	51	17	29	20
	Combination treatment	51	18	35	24
VSI: Blood volume (arbitrary units)	Control	282	303	—	331
	Zoledronic acid	287	252	—	237
	Sunitinib malate	290	174	—	178
	Combination treatment	306	182	—	177
VSI: Vessel size index (μm)	Control	50	41	—	44
	Zoledronic acid	51	52	—	56
	Sunitinib malate	41	64	—	75
	Combination treatment	43	58	—	69

B

Imaging method	Comparison	*P* value			
		Day 0	Day 5	Day 15	Day 25
VCT: Volume of osteolysis	Zoledronic acid vs control	0.633	0.829	0.408	0.203
	Sunitinib malate vs control	0.762	0.696	0.173	0.012
	Combination treatment vs control	0.965	0.274	0.015	0.002
	Zoledronic acid vs sunitinib malate	0.959	1.041	0.645	0.328
	Zoledronic acid vs combination treatment	0.721	0.328	0.328	0.105
	Sunitinib malate vs combination treatment	0.878	0.574	0.574	0.574
MRI: Volume of soft-tissue component	Zoledronic acid vs control	0.573	0.897	0.762	0.515
	Sunitinib malate vs control	0.829	0.573	0.083	0.006
	Combination treatment vs control	0.762	0.122	0.027	0.001
	Zoledronic acid vs sunitinib malate	0.959	0.382	0.105	0.021
	Zoledronic acid vs combination treatment	0.574	0.130	0.010	0.002
	Sunitinib malate vs combination treatment	0.721	0.798	0.798	0.442
DWI: Apparent diffusion coefficient	Zoledronic acid vs control	0.515	0.573	0.315	0.965
	Sunitinib malate vs control	0.408	0.237	0.012	0.027
	Combination treatment vs control	0.101	0.515	0.054	0.083

(*Continued on the following page*)

Table 1. Study results from longitudinal imaging (A, mean values of imaging parameters; B, comparison between study groups) and histology (C) (Cont'd)

B

Imaging method	Group	*P* value			
		Day 0	Day 5	Day 15	Day 25
	Zoledronic acid vs sunitinib malate	1.040	0.645	0.065	0.065
	Zoledronic acid vs combination treatment	0.382	0.160	0.235	0.195
	Sunitinib malate vs combination treatment	0.235	0.015	0.279	0.382
DCE-MRI: Amplitude	Zoledronic acid vs control	0.897	0.016	0.043	0.016
	Sunitinib malate vs control	0.573	0.004	0.001	<0.001
	Combination treatment vs control	0.274	0.009	0.003	0.002
	Zoledronic acid vs sunitinib malate	0.645	0.328	0.105	0.005
	Zoledronic acid vs combination treatment	0.328	0.083	0.038	0.021
	Sunitinib malate vs combination treatment	0.959	0.279	0.279	0.645
DCE-MRI: Exchange rate constant	Zoledronic acid vs control	0.237	0.274	0.572	0.012
	Sunitinib malate vs control	0.965	0.002	0.027	<0.001
	Combination treatment vs control	0.965	0.009	0.101	0.006
	Zoledronic acid vs sunitinib malate	0.161	0.021	0.279	0.038
	Zoledronic acid vs combination treatment	0.194	0.021	0.442	0.038
	Sunitinib malate vs combination treatment	0.721	0.959	0.574	0.195
VSI: Blood volume	Zoledronic acid vs control	0.792	0.065	—	<0.001
	Sunitinib malate vs control	0.621	0.001	—	<0.001
	Combination treatment vs control	0.621	0.008	—	<0.001
	Zoledronic acid vs sunitinib malate	0.755	0.001	—	0.015
	Zoledronic acid vs combination treatment	0.662	0.043	—	0.130
	Sunitinib malate vs combination treatment	0.505	0.721	—	0.645
VSI: Vessel size index	Zoledronic acid vs control	1.069	0.132	—	0.121
	Sunitinib malate vs control	0.354	0.003	—	0.001
	Combination treatment vs control	0.435	0.008	—	0.012
	Zoledronic acid vs sunitinib malate	0.081	0.020	—	0.083
	Zoledronic acid vs combination treatment	0.081	0.754	—	0.195
	Sunitinib malate vs combination treatment	0.645	0.721	—	0.505

C

Histology	Collagen IV*		SMA*		Vessel diameter	
	%	*P*	%	*P*	μm	*P*
Control	3.48	—	0.95	9.84	—	
Zoledronic acid	2.59	0.02	1.05	0.902	10.89	0.148
Sunitinib malate	0.91	<0.001	0.89	0.456	18.33	0.001
Combination treatment	0.87	<0.001	0.96	0.683	17.27	0.001

*The given values for collagen IV and SMA are expressed as positive area fractions in percent.

density (MVD) was determined by calculating positive area fractions of collagen IV. When comparing immunostainings for CD31 and collagen IV to determine the MVD, a positive correlation was observed in soft-tissue components of bone metastases (data not shown).

Statistical analyses

For each animal, absolute values for osteolytic lesion and soft-tissue component volumes, A, k_{ep}, ADC, VI, and BV were plotted versus time after initiation of therapy. After quantitative histologic analysis, values of the positive area fractions as well as the vessel diameters were compared. For statistical comparisons, the respective values were compared between the control and treatment groups as well as between the treatment groups using the two-sided Wilcoxon test; P values <0.05 were considered significant.

Results

Flat-panel VCT and MRI

After ZA monotherapy, decreased values for the volumes of osteolytic lesions and soft-tissue components were

observed at days 5, 15, and 25 after initiation of therapy as compared with controls, but differences did not reach statistical significance (Fig. 1A and B; Table 1A and B). SM monotherapy and combination treatment resulted in a significant reduction of osteolytic lesion and soft-tissue component volumes at day 25 and additionally at day 15 for the combination treatment group compared with controls (Fig. 1A and B; Table 1A and B). Representative figures of osteolytic lesions and soft-tissue components of the control and treatment groups are shown in Fig. 2.

Diffusion-weighted imaging

Although ADC values in animals treated with ZA were higher than those of controls at each time point after initiation of therapy, no statistically significant differences between the groups were observed (Figs. 1C and 2A-B; Table 1A and B). However, significantly increased ADC values were found in rats after SM monotherapy at days 15 and 25 as compared with controls, but not after combination therapy (Figs. 1C and 2C-D; Table 1A and B).

Dynamic contrast-enhanced MRI

ZA monotherapy resulted in significantly decreased *A* values at all observed time points after initiation of therapy as compared with controls, whereas an even greater reduction was observed after SM monotherapy and combination treatment at each time point of the observation period (Fig. 3A; Table 1A and B). Values for k_{ep} were significantly decreased in animals after ZA treatment than in untreated rats at day 25 (Fig. 3B; Table 1A and B). Furthermore, significantly decreased k_{ep} values were observed at days 5, 15, and 25 after SM monotherapy as well as at days 5 and 25 after combination treatment in comparison with controls (Fig. 3B; Table 1A and B). Representative color maps from bone metastases of the control and treatment groups are shown in Fig. 4.

Vessel size imaging

Compared with controls, significantly decreased values for the BV were observed in animals treated with ZA, SM, and the combination at day 25 as well as with SM and

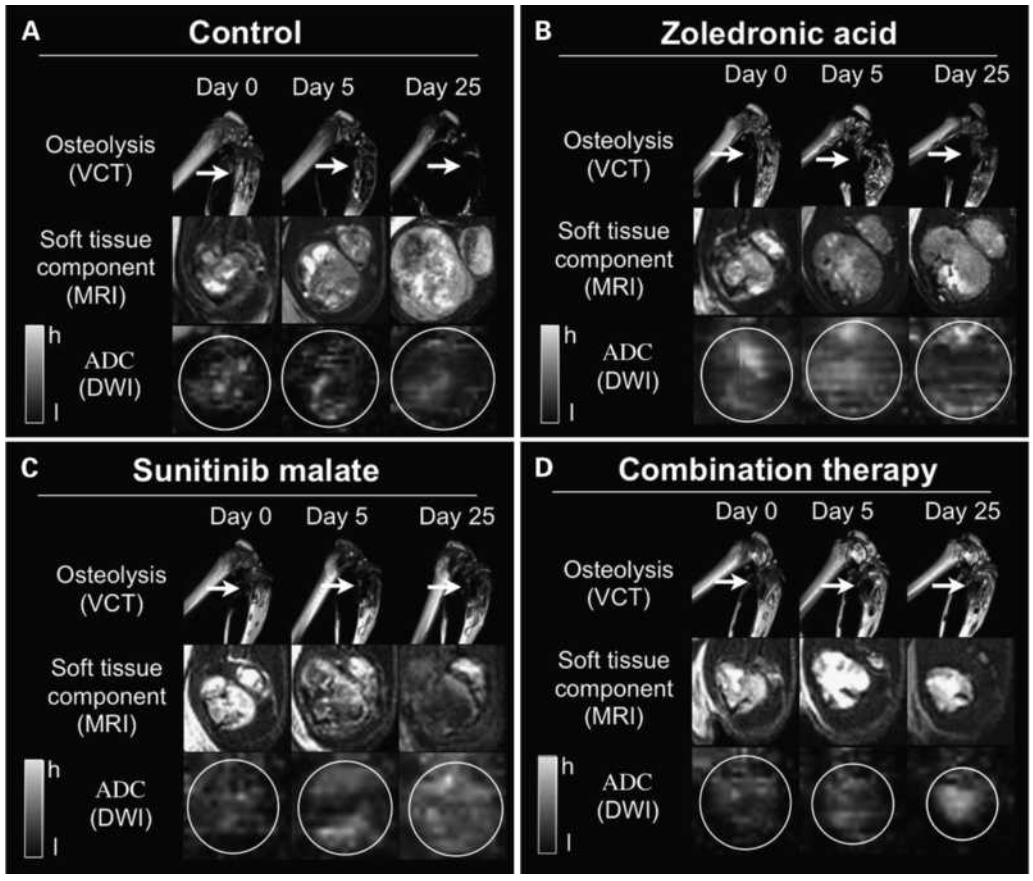

Fig. 2. A to D, morphology of experimental bone metastases as imaged by VCT and MRI as well as ADC maps at days 0, 5, and 25 (A, untreated control; B, treatment with ZA; C, treatment with SM; D, combination therapy). Top rows, three-dimensional reconstructions of osteolytic lesions (arrows) in the hind leg of rats as imaged with VCT. Middle rows, axial slices from T2 weighted magnetic resonance images of the hyperintense soft-tissue lesions of bone metastases as compared with hypointense muscle tissue surrounding the metastases. Bottom rows, ADC maps in axial orientation ranging from high (h; white) to low (l; black) values (white circles delineate bone metastases).

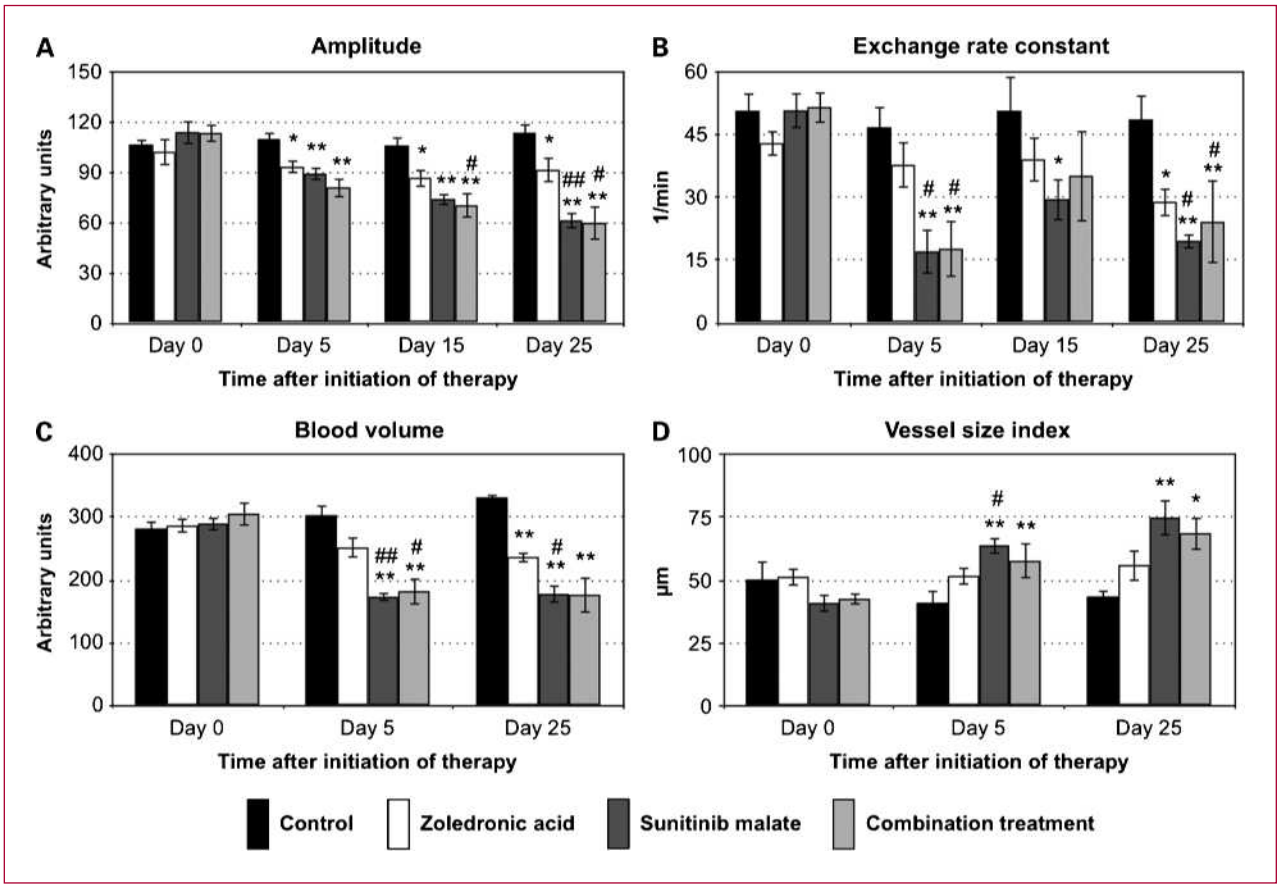

Fig. 3. A to D, study results of parameters acquired with DCE-MRI and VSI from experimental bone metastases between days 0 and 25 after initiation of treatment. A and B, amplitude (A) and exchange rate constant (B) as assessed with DCE-MRI. C and D, blood volume (C) and vessel size index (D) as assessed with VSI. Bars, SE. *, compared with the control group; #, compared with the ZA monotherapy group (* and #, $P < 0.05$; ** and ##, $P < 0.01$).

combination treatment additionally at day 5 (Fig. 3C; Table 1A and B). Values of the VI after ZA monotherapy were higher than in untreated controls, but were not significantly different between the groups (Fig. 3D; Table 1A and B). During SM mono- and combination therapies, significantly increased values of the VI could be calculated at days 5 and 25 as compared with controls (Fig. 3D; Table 1A and B). Representative color maps from bone metastases of the control and treatment groups are shown in Fig. 4.

Comparison of treatment groups

When comparing rats receiving ZA monotherapy with animals receiving SM monotherapy or combination treatment, significant differences between the groups for all vascular parameters (A, k_{ep}, BV, and VI; Fig. 3A-D; Table 1B) and for soft-tissue component volumes (Fig. 1B; Table 1B) were observed, but not for osteolytic lesion volumes (Fig. 1A; Table 1B) or ADC values (Fig. 1C; Table 1B). Comparison of rats receiving SM monotherapy and combination treatment resulted in significantly lower ADC values in animals of the combination treatment group at day 5 after initiation of therapy (Fig. 1C; Table 1B). However, no additional significant differences were observed for any parameter acquired by noninvasive imaging between these groups (Table 1B).

Histology

Immunofluorescent analysis in control animals revealed multiple irregular vessels with small diameters indicated by collagen IV staining, which were not colocalized with smooth muscle actin (SMA), along with few larger vessels showing collagen IV/SMA colocalization (collagen IV/SMA ratio, 3.5:1.0; Fig. 5A; Table 1C). After ZA monotherapy, the MVD as derived from collagen IV staining was significantly decreased when compared with controls (Fig. 5B; Table 1C). In these animals, particularly larger vessels showed an increased collagen IV/SMA colocalization (collagen IV/SMA ratio, 2.6:1.1; Fig. 5B; Table 1C) after ZA monotherapy in comparison with controls. In animals treated with SM mono- and combination therapies, decreased MVD ($P < 0.01$) and collagen IV/SMA ratios (0.9:0.9 for SM monotherapy and 0.9:1.0 for combination therapy) and increased mean vessel diameters ($P < 0.01$) were observed as compared with controls (Fig. 5C and D; Table 1C).

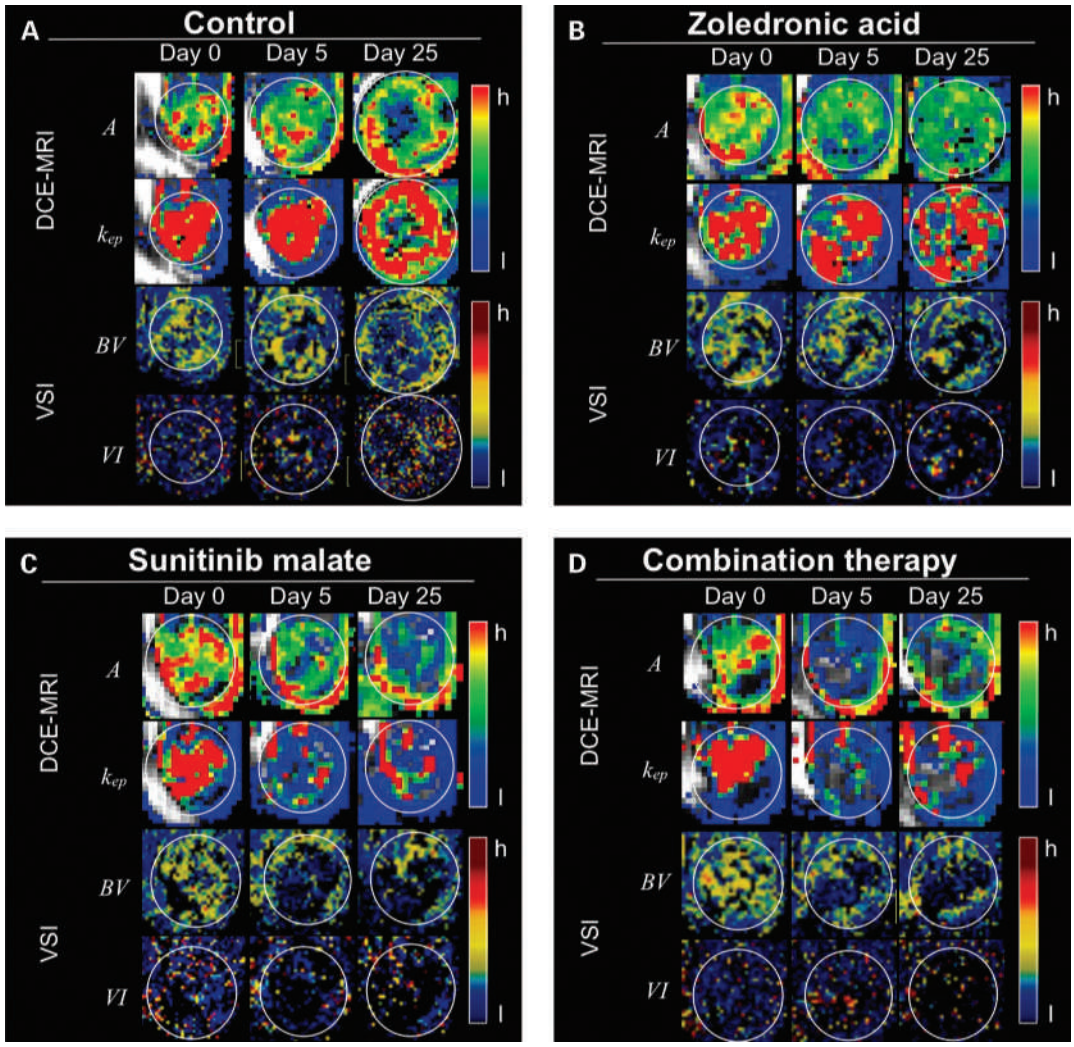

Fig. 4. A to D, color maps of experimental bone metastases as imaged by DCE-MRI and VSI at days 0, 5, and 25 (A, untreated control; B, treatment with ZA; C, treatment with SM; D, combination therapy). First rows, *A*; second rows, k_{ep}; third rows, BV; fourth rows, VI. Color maps in axial orientation (white circles delineate bone metastases) for all parameters ranging from high (h; red) to low values (l; blue).

Discussion

The aim of this longitudinal study was to assess the antiangiogenic, antiresorptive, and antitumor effects of ZA and SM in experimental breast cancer bone metastases using noninvasive imaging methods.

According to the two-compartment model of Brix, changes in the vasculature of bone metastases could be assessed noninvasively and *in vivo* by the DCE-MRI parameters *A* and k_{ep} (20–22). In these osseous lesions, we characterized the antiangiogenic properties of ZA for the first time and observed a decrease of *A* as early as 5 days after the initial application of ZA in comparison with control rats. This finding indicated an early reduction of regional blood volume after ZA treatment corresponding with a decreased MVD observed by immunofluorescent analysis, which was most probably a consequence of the previously described inhibition of endothelial cell proliferation and vessel sprouting on ZA treatment (8, 9, 23). Furthermore, a significant decrease of k_{ep} under ZA monotherapy was observed at the end of the observation time in bone metastases, indicating reduced vessel permeability as compared with controls. This change in k_{ep} was in accordance to a more pronounced pericyte coverage of the remaining vasculature due to vessel maturation.

In breast cancer bone metastases of animals treated with SM monotherapy and combination treatment, significantly decreased values for *A* and k_{ep} were assessed at almost

each time point of the observation period. Compared with the above-mentioned results on ZA treatment, these findings indicated an even stronger decrease in blood volume and vessel permeability in line with the findings from immunohistology revealing vessel regression and maturation on SM monotherapy and combination treatment. These vascular changes after inhibiting the VEGF-VEGF receptor axis have been found in various preclinical and clinical studies in solid tumors, but such changes have not been observed and analyzed in bone metastases (24–27).

Differences in mean vessel size and regional blood volume of vasculature can be assessed by alterations in T2 and T2* relaxation times induced by superparamagnetic iron oxide nanoparticles using VSI (16). Applying this technique to bone metastases, the significant decrease in blood volume after treatment with ZA, SM, and the combination therapy corresponded to a significant decrease of DCE-MRI parameter *A* as an alternative measurement for regional blood volume. After SM monotherapy and combination treatment, significantly increased vessel size indices were observed, which was in line with a recent study showing increased mean vessel size diameters and vessel regression in subcutaneous tumors on SM treatment (14). When comparing vessel diameters determined by VSI and histology, an overestimation of mean vessel calibers by noninvasive imaging was observed, which has been described before (16, 28). In our study, small immature vessels most probably regressed due to VEGF inhibition, whereas bigger mature vessels persisted leading to an overall larger mean vessel diameter (29). Taken together, the results of significant changes in *A*, k_{ep}, BV, and VI values as assessed noninvasively in experimental breast cancer bone metastases indicate vessel remodeling including small vessel regression and vessel maturation after SM treatment. For ZA, antiangiogenic properties such as the inhibition of new vessel formation leading to a decreased regional blood volume have not been shown in bone metastases. However, these findings have to be confirmed in patients suffering from malignant bone lesions (e.g., skeletal metastases or multiple myeloma; ref. 30).

Besides the antiangiogenic effects of ZA and SM in our model, we observed an inhibition of bone resorption with these treatments. Also, previous reports described antiresorptive effects after antiangiogenic therapy, indicating a link between angiogenesis and osteolytic activity in bone metastases (4, 31, 32). A probable explanation for this phenomenon is the recently discovered fact that small capillaries are in close vicinity of bone remodeling units, where capillaries route pre-osteoclasts to the site of bone resorption (5). As a consequence, in particular, the disruption of small tumor vessels including capillaries, as observed in our study after SM treatment, might have impaired the migration and maturation of osteoclasts resulting in antiresorptive effects. Another possible mechanism for the inhibition of osteoclastic bone resorption by these drugs might be the direct inhibition of VEGF- and platelet-derived growth factor–associated effects. As an explanation, VEGF, platelet-derived growth factor, as well as the respective receptors were reported to be expressed by tumor and stroma cells in bone metastases and their interaction has been associated with osteoclast-mediated osteolysis (20, 33–36).

SM and ZA treatment resulted not only in antiangiogenic and antiresorptive effects but also had an effect

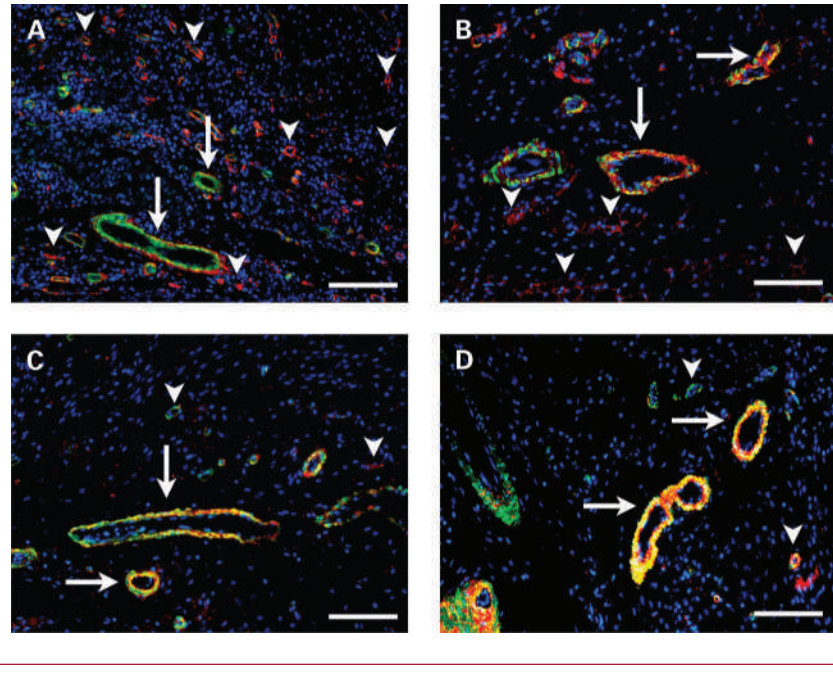

Fig. 5. A to D, immunofluorescent analysis of experimental bone metastases stained for SMA (green), collagen IV (red), and 4′,6-diamidino-2-phenylindole (blue) of a control rat (A) and rats of the treatment groups (B, ZA; C, SM; D, combination treatment). Arrowheads, small tumor vessels; arrows, larger vessels. Magnification, 20-fold; bar, 100 μm.

on the soft-tissue component of bone metastases consisting of tumor cells and stroma as assessed by morphologic MRI and DWI. The ADC from DWI was associated with the cellularity of tissues and introduced as an imaging biomarker for early detection of antitumor effects in prostate cancer bone metastases (18, 37, 38). In our study, treatment with SM alone or in combination with ZA significantly decreased the volumes of the soft-tissue component and increased ADC values, indicating a reduction in cellularity. Also, ZA monotherapy decreased the tumor volume and increased ADC values in comparison with controls, but changes did not reach significance. These findings suggest a strong antitumor efficacy of SM and, to a lesser extent, of ZA monotherapy as assessed with DWI and morphologic MRI.

When comparing treatment groups in our study, antiangiogenic and antitumor effects were more pronounced in rats receiving SM monotherapy compared with rats receiving ZA monotherapy. However, the combined therapy with ZA and SM was not beneficial over SM monotherapy because no statistically significant advantage of the combination treatment was found for any parameter assessed by noninvasive imaging in our study. During treatment, even significantly lower ADC values indicating increased cellularity were found for the combination treatment as compared with SM monotherapy. Further studies with different dosages of SM and ZA should be conducted to analyze dose-dependent effects resulting from mono- and combination therapies with these drugs.

In patients with bone metastases, assessment of treatment response is pivotal in clinical practice (15). According to the most recent version of the Response Evaluation Criteria in Solid Tumors, measurements of the osteolytic lesion size by CT and the soft-tissue component by MRI are proposed methods to determine changes in the morphology of osseous lesions (17). However, a change in lesion size of bone metastases is usually assessed weeks or months after initiation of treatment because a change of morphology is slow, particularly in bone (39). According to our results, it seems worthwhile validating the noninvasive imaging parameters from DCE-MRI and VSI as potential early markers for assessment of treatment response after bisphosphonate and antiangiogenic treatments in patients with bone metastases by capturing vascular changes before a reduction in lesion size becomes apparent.

Here, we report on vessel remodeling in response to ZA, which is even more pronounced after SM treatment, in experimental breast cancer bone metastases as assessed noninvasively by quantitative imaging parameters from DCE-MRI and VSI. In our longitudinal study, these vascular changes preceded the antiresorptive and antitumor effects of ZA and SM in bone lesions, highlighting the imaging of angiogenesis in bone metastases as a valuable method for early and quantitative assessment of response after bisphosphonate and antiangiogenic treatments. Further clinical studies are required to confirm the proposed link between antiangiogenic effects and the inhibition of osteolysis of these drugs in patients with malignant bone lesions.

Disclosure of Potential Conflicts of Interest

No potential conflicts of interest were disclosed.

Acknowledgments

We thank Karin Leotta and Renate Bangert for excellent technical assistance as well as Bram Stieltjes, Frederik Laun, and Dirk Simon for their support and valuable discussions about DWI techniques. We also thank Pfizer for providing SU-11248, Guerbet for supplying Sinerem, and the Deutsche Forschungsgemeinschaft (SFB-TR23) for their financial support.

Grant Support

Tobias Bäuerle and Dorde Komljenovic (Deutsche Forschungsgemeinschaft, SFB-TR23).

The costs of publication of this article were defrayed in part by the payment of page charges. This article must therefore be hereby marked *advertisement* in accordance with 18 U.S.C. Section 1734 solely to indicate this fact.

Received 11/03/2009; revised 03/02/2010; accepted 04/22/2010; published OnlineFirst 06/08/2010.

References

1. Voorzanger-Rousselot N, Juillet F, Mareau E, Zimmermann J, Kalebic T, Garnero P. Association of 12 serum biochemical markers of angiogenesis, tumour invasion and bone turnover with bone metastases from breast cancer: a cross-sectional and longitudinal evaluation. Br J Cancer 2006;95:506–14.
2. Chavez-Macgregor M, Aviles-Salas A, Green D, Fuentes-Alburo A, Gomez-Ruiz C, Aguayo A. Angiogenesis in the bone marrow of patients with breast cancer. Clin Cancer Res 2005;11:5396–400.
3. van der Pluijm G, Sijmons B, Vloedgraven H, Deckers M, Papapoulos S, Lowik C. Monitoring metastatic behavior of human tumor cells in mice with species-specific polymerase chain reaction: elevated expression of angiogenesis and bone resorption stimulators by breast cancer in bone metastases. J Bone Miner Res 2001;16:1077–91.
4. Peyruchaud O, Serre CM, NicAmhlaoibh R, Fournier P, Clezardin P. Angiostatin inhibits bone metastasis formation in nude mice through a direct anti-osteoclastic activity. J Biol Chem 2003; 278:45826–32.
5. Andersen TL, Sondergaard TE, Skorzynska KE, et al. A physical mechanism for coupling bone resorption and formation in adult human bone. Am J Pathol 2009;174:239–47.
6. Daubine F, Le Gall C, Gasser J, Green J, Clezardin P. Antitumor effects of clinical dosing regimens of bisphosphonates in experimental breast cancer bone metastasis. J Natl Cancer Inst 2007;99:322–30.
7. Santini D, Vincenzi B, Galluzzo S, et al. Repeated intermittent low-dose therapy with zoledronic acid induces an early, sustained, and long-lasting decrease of peripheral vascular endothelial growth factor levels in cancer patients. Clin Cancer Res 2007;13:4482–6.
8. Wood J, Bonjean K, Ruetz S, et al. Novel antiangiogenic effects of the bisphosphonate compound zoledronic acid. J Pharmacol Exp Ther 2002;302:1055–61.
9. Yamada J, Tsuno NH, Kitayama J, et al. Anti-angiogenic property of zoledronic acid by inhibition of endothelial progenitor cell differentiation. J Surg Res 2009;151:115–20.
10. Wedge SR, Jürgensmeier JM. VEGFR receptor tyrosine kinase inhibitors for the treatment of cancer. Berlin, Heidelberg, New York: Springer; 2008, p. 395–425.

11. Abrams TJ, Murray LJ, Pesenti E, et al. Preclinical evaluation of the tyrosine kinase inhibitor SU11248 as a single agent and in combination with *standard of care* therapeutic agents for the treatment of breast cancer. Mol Cancer Ther 2003;2:1011–21.
12. Murray LJ, Abrams TJ, Long KR, et al. SU11248 inhibits tumor growth and CSF-1R-dependent osteolysis in an experimental breast cancer bone metastasis model. Clin Exp Metastasis 2003; 20:757–66.
13. Kiessling F, Jugold M, Woenne EC, Brix G. Non-invasive assessment of vessel morphology and function in tumors by magnetic resonance imaging. Eur Radiol 2007;17:2136–48.
14. Zwick S, Strecker R, Kiselev V, et al. Assessment of vascular remodeling under antiangiogenic therapy using DCE-MRI and vessel size imaging. J Magn Reson Imaging 2009;29:1125–33.
15. Bäuerle T, Semmler W. Imaging response to systemic therapy for bone metastases. Eur Radiol 2009;19:2495–507.
16. Tropres I, Grimault S, Vaeth A, et al. Vessel size imaging. Magn Reson Med 2001;45:397–408.
17. Eisenhauer EA, Therasse P, Bogaerts J, et al. New response evaluation criteria in solid tumours: revised RECIST guideline (version 1.1). Eur J Cancer 2009;45:228–47.
18. Lee KC, Sud S, Meyer CR, et al. An imaging biomarker of early treatment response in prostate cancer that has metastasized to the bone. Cancer Res 2007;67:3524–8.
19. Bäuerle T, Adwan H, Kiessling F, Hilbig H, Armbruster FP, Berger MR. Characterization of a rat model with site-specific bone metastasis induced by MDA-MB-231 breast cancer cells and its application to the effects of an antibody against bone sialoprotein. Int J Cancer 2005; 115:177–86.
20. Bäuerle T, Hilbig H, Bartling S, et al. Bevacizumab inhibits breast cancer induced osteolysis, surrounding soft tissue metastasis, and angiogenesis in rats as visualized by VCT and MRI. Neoplasia 2008;10:511–20.
21. Bäuerle T, Bartling S, Berger M, et al. Imaging anti-angiogenic treatment response with DCE-VCT, DCE-MRI and DWI in an animal model of breast cancer bone metastasis. Eur J Radiol 2010;73:280–7.
22. Brix G, Semmler W, Port R, Schad LR, Layer G, Lorenz WJ. Pharmacokinetic parameters in CNS Gd-DTPA enhanced MR imaging. J Comput Assist Tomogr 1991;15:621–8.
23. Cooper CR, Satcher RA, Gurski LA. Mechanism of metastasis to bone: the role of bone marrow endothelium. London: Springer; 2009, p. 57–72.
24. Tong RT, Boucher Y, Kozin SV, Winkler F, Hicklin DJ, Jain RK. Vascular normalization by vascular endothelial growth factor receptor 2 blockade induces a pressure gradient across the vasculature and improves drug penetration in tumors. Cancer Res 2004;64:3731–6.
25. Winkler F, Kozin SV, Tong RT, et al. Kinetics of vascular normalization by VEGFR2 blockade governs brain tumor response to radiation: role of oxygenation, angiopoietin-1, and matrix metalloproteinases. Cancer Cell 2004;6:553–63.
26. Willett CG, Boucher Y, di Tomaso E, et al. Direct evidence that the VEGF-specific antibody bevacizumab has antivascular effects in human rectal cancer. Nat Med 2004;10:145–7.
27. Jain RK. Molecular regulation of vessel maturation. Nat Med 2003; 9:685–93.
28. Kiselev VG, Strecker R, Ziyeh S, Speck O, Hennig J. Vessel size imaging in humans. Magn Reson Med 2005;53:553–63.
29. Benjamin LE, Golijanin D, Itin A, Pode D, Keshet E. Selective ablation of immature blood vessels in established human tumors follows vascular endothelial growth factor withdrawal. J Clin Invest 1999; 103:159–65.
30. Ribatti D, Nico B, Vacca A. Importance of the bone marrow microenvironment in inducing the angiogenic response in multiple myeloma. Oncogene 2006;25:4257–66.
31. Weber MH, Lee J, Orr FW. The effect of Neovastat (AE-941) on an experimental metastatic bone tumor model. Int J Oncol 2002; 20:299–303.
32. Engebraaten O, Trikha M, Juell S, Garman-Vik S, Fodstad O. Inhibition of in vive tumour growth by the blocking of host α(v)β3 and αII (b)β3 integrins. Anticancer Res 2009;29:131–7.
33. Lev DC, Kim SJ, Onn A, et al. Inhibition of platelet-derived growth factor receptor signaling restricts the growth of human breast cancer in the bone of nude mice. Clin Cancer Res 2005;11:306–14.
34. Aldridge SE, Lennard TW, Williams JR, Birch MA. Vascular endothelial growth factor acts as an osteolytic factor in breast cancer metastases to bone. Br J Cancer 2005;92:1531–7.
35. Engsig MT, Chen QJ, Vu TH, et al. Matrix metalloproteinase 9 and vascular endothelial growth factor are essential for osteoclast recruitment into developing long bones. J Cell Biol 2000;151:879–89.
36. Niida S, Kaku M, Amano H, et al. Vascular endothelial growth factor can substitute for macrophage colony-stimulating factor in the support of osteoclastic bone resorption. J Exp Med 1999;190:293–8.
37. Lee KC, Bradley DA, Hussain M, et al. A feasibility study evaluating the functional diffusion map as a predictive imaging biomarker for detection of treatment response in a patient with metastatic prostate cancer to the bone. Neoplasia 2007;9:1003–11.
38. Lyng H, Haraldseth O, Rofstad EK. Measurement of cell density and necrotic fraction in human melanoma xenografts by diffusion weighted magnetic resonance imaging. Magn Reson Med 2000;43:828–36.
39. Hamaoka T, Madewell JE, Podoloff DA, Hortobagyi GN, Ueno NT. Bone imaging in metastatic breast cancer. J Clin Oncol 2004; 22:2942–53.